ISSN 0915-633X

NATIONAL INSTITUTE FOR FUSION SCIENCE

A Detection Method of Negative Pionlike Particles from a H_2 Gas Descharge Plasma

J. Uramoto

(Received - Dec. 5, 1995)

NIFS-400 Feb. 1996

RESEARCH REPORT
NIFS Series

NAGOYA, JAPAN

A detection method of negative pionlike particles from a H_2 gas discharge plasma

Jōshin URAMOTO

National Institute for Fusion Science

Nagoya 464-01, Japan

Abstract

The negative pionlike particles π^- penetrate a metal (or insulator) plate if positive ions produced secondarily by H^- ions, diffuse to the back of the plate. Thus, the π^- particles are not detected by a usual beam collector of mass analyzer using a metal plate. In order to detect the π^- particles, we must interrupt the diffusion of the positive ions to the back of the beam collector while the π^- particles are confined inside the beam collector and changed into a multiplied electron current.

Keywords: negative pionlike particle π^-, beam collector,

positive ion diffusion

It has been reported[1),2)] already that negative pionlike particles are generated through some interactions between the electron bunch and the positive ion bunch. Then, it has been pointed out[2,3)] that the negative pionlike (π^-) particles penetrate a metal plate if positive ions exist behind the metal plate. Inversely, if the positive ions do not exist behind it, we can consider that the π^-particles do not penetrate it and will be confined inside it during their life times. This physical character of the π^- particles become very important when we try to detect the π^- particles by a beam collector of the magnetic mass analyzer using a metal plate.

In this paper, a relation between the above character and the positive ions will be investigated more precisely while a method of effective detection is found for the π^- particles extracting from the H_2 gas discharge plasma.

A schematic diagram of the experimental apparatus is shown in Fig. 1. The apparatus is constructed from a H_2 gas discharge plasma in magnetic fields, three extraction electrodes (with an aperture of 3 mm in diameter) to extract some negatively charged particles and a magnetic mass analyzer (90° deflection-type).

More precise schematic diagrams of the magnetic mass analyzer and the extraction electrodes are shown in Fig. 1 MA and Fig 2 MA. The (fringe) magnetic field distribution is shown in Fig. 3 MA also.

An electron acceleration-type sheet plasma[4)] is produced to generate H^- or D^- ions effectively and in wide area. That is, the discharge (cylindrical) plasma flow of about 1 cm in diameter is transformed into a sheet plasma flow of about 3 mm in thickness and about 20 cm in width, while the electron components in the initial discharge plasma are accelerated near 80 eV. The sheet plasma flow passes through the electron acceleration anode (12 in Fig. 1) and enters the main chamber (50 cm long). The electron components in the sheet plasma are reflected by the end plate which is electrically floated. A uniform magnetic field of about 50 gauss is applied along the sheet plasma flow in the main chamber where the H_2 gas pressure is about 1.5×10^{-3} Torr. The electron acceleration anode current I_A is 20A and about 60% of I_A enters the main chamber. A distance between the sheet plasma center and the first extraction electrode (L) is 7.5 cm. The plasma density in the center of the sheet plasma is about 10^{11}/cc and the electron temperature is about 20 eV. The positive ion density in front of the first extraction electrode is estimated to be about 7.5×10^9/cc

from a positive ion saturation current as H_3^+, while the electron density from the Langmuir probe characteristic is about 8.2×10^8/cc and the electron temperature is about 3.0 eV. That is, the electron density in front of the first extraction electrode is reduced near 1/10 of the positive ion density. It is estimated from the beam collector current of the magnetic analyzer that the extracted H^- ion current density is comparable to the extracted H_3^+ ion current density.

The negatively charged particles extracted from the H_2 or D_2 gas discharge plasma, are injected into the ordinary magnetic mass analyzer (MA) through the slit (3 mm × 1 cm) while each mass of the negatively charged particle is estimated by the following relations: From the analyzing magnetic field B_M where the negative current to the beam collector BC shows a peak, the curvature radius r of the mass analyzer and the extraction (acceleration) voltage V_E, we can estimate the mass m of the negatively charged particle by,

$$m = \frac{Ze\,(B_M r)^2}{2V_E}$$

$$= \frac{8.8 \times 10^{-2} Z\,(B_M r)^2\, m_e}{V_E}, \quad \cdots\cdots (1)$$

where e is the electron charge, B_M is in gauss unit, r is in cm unit, V_E is in volt unit and m_e is the electron mass and Z is the charge number. For the curvature radius $r = 4.3$ cm of this mass analyzer, the Eq. (1) is rewritten by

$$m = \frac{1.63\, Z\, B_M^2}{V_E} m_e. \quad \cdots\cdots (2)$$

In the extraction of negatively charged particles, the first extraction electrode (L) is electrically floated, whose potential V_L is about –15V with respect to the electron acceleration anode (12 in Fig. 1). A potential V_M of the second extraction electrode (M) is kept at 300V. The potential V_E of the final extraction electrode (E) is 800V.

In the first experiment, the back space of the beam collector is shielded perfectly from the injection of positive ions as shown in Fig. 2 (A). That is, the back space is surrounded by metal plates and insulators. The dependences of the negative current Γ^- to the beam collector on the analyzing magnetic field B_M are shown in Fig. 2 (B). The first peak of Γ^- corresponding to the π^-

particles and the second peak corresponding to the H^- ions are observed clearly. That is, for V_E = 800V and $B_M \approx 353$ gauss of the first peak, we obtain $m_1 \approx 253\ m_e$ (near the typical π^- mass) from Eq. (2), assuming that Z = 1. Similarly, for V_E = 800V and $B_M \approx 940$ gauss, we obtain $m_2 \approx 1800\ m_e$ (near the H^- ion mass).

The positive ion current to the beam collector is about 0.02 μA for the beam collector area (0.5 cm^2), which is measured by giving a deep negative bias voltage (V_{BC} = –350V) to the beam collector and under the analyzing magnetic field corresponding to the first peak current of I^-. The positive ions may be produced secondarily from the extracting H^- ions. In the back space of the beam collector of this first experiment, the positive ion current is not observed.

In the second experiment, the positive ions diffuse to the back space of the beam collector while the back space is open as shown in Fig. 3 (A). Then, the dependences of the negative current I^- on B_M are shown in Fig. 3 (B). The first peak of I^- corresponding to the π^- particles disappears while only the second peak of I^- corresponding to the H^- ions appears.

As the third experiment, in addition to the first experiment of Fig. 2 (A), a Cu plate of 0.5 mm in thickness is put partially in front of the beam collector as shown in Fig. 4 (A). The dependences of I^- on B_M are shown in Fig. 4 (B). Then, only the first peak of I^- corresponding to the π^- particles appears. In this case, it is observed clearly the positive ions diffuse behind the partial Cu plate. As discussed late, the above experimental fact shows that a large part of the π^- particles penetrate the Cu plate if the positive ions exist behind the Cu plate.

As the forth experiment, in addition to the first experiment, a long Cu plate is put to shield perfectly from diffusion of the positive ions to the region of the beam collector, as shown in Fig. 5 (B). Then, both the first peak and the second peak of I^- disappear. This fact shows that the π^- particles can not penetrate if the positive ions do not exist behind the Cu plate. In fact, the positive ion current is not collected by the beam collector even if the large negative bias voltage is given.

Usually, a diffusion of back ground electrons inside of the mass analyzer may be induced as an ambipolar diffusion due to the positive ions. Then, a negative current I^- of the electrons to the beam collector may appear. Here, a difference between the penetration phenomenon of the metal plate and the above electron diffusion must be clarified. In the second experiment of Figs. 3 (A) and 3 (B), we do not detect the negative (pionlike) current peak to the beam collector though the

positive ions exist around the beam collector. If the first peak of the negative current Γ^- is generated by the electron diffusion, the first peak must appear also in this case of Figs. 3 (A) and 3 (B). However, we do not observe the first peak. Therefore, we conclude that the first peak of Γ^- is not generated by the electron diffusion. Obviously, when the positive ions behind the beam collector are removed, the negative pionlike current peak appears clearly as seen in the first experiment of Figs. 2 (A) and 2 (B).

In the third experiment of Figs. 4 (A) and 4 (B), the beam collector is interrupted partially by the metal plate and the positive ions diffuse in front of the beam collector while a large part of the negative current peak corresponding to the π^- particles, appears clearly also. In the forth experiment, the beam collector is interrupted perfectly and the positive ions can not diffuse in front of the beam collector while the negative current peak disappears.

From these experimental facts, we can conclude that the π^- particles penetrate the metal plate (or the insulator plate also) if the positive ions diffuse to the back of the metal plate or the insulator plate. Inversely, the negative current corresponding to the π^- particles can be detected clearly by removing or reducing the positive ions behind the beam collector.

When the positive ions behind the beam collector are removed, the π^- particles can not penetrate the beam collector (metal plate) and will be confined inside the beam collector. As a result, a large electron current generates between the beam collector and the mass analyzer body.

Here, we consider that the π^- particles inside the beam collector change into electrons which generate the large electron current.

References

1) J. Uramoto: National Institute of Fusion Science, Nagoya, Japan-Research Report, NIFS-277 (1994).

2) J. Uramoto: NIFS-377 (1995).

3) J. Uramoto: NIFS-350 (1995).

4) J. Uramoto: Journal of the vacuum society of Japan, **37** (1994) 507 in Japanese.

Appendix

An arrangement of insulators around the beam collector is shown in Fig. A1 (A), which was used before this paper and was not investigated precisely. Dependences of the negative current I^- to the beam collector on the analyzing magnetic field B_M, are shown in Fig. A2 (B) correspondingly to the above arrangement.

Another arrangement of insulators is shown in Fig. A2 (A). The dependences of the negative current I^- are shown in Fig. A2 (B). There, the first current peak of I^- corresponding to the π^- particles disappears as the positive ions come from the left side of the beam collector.

In Fig. A3, the most practical arrangement of the insulator (Ins) for the dection of the π^- particles is shown, where the diffusion of the positive ions to the back space of the beam collector is interrupted perfectly and easily.

Figure Captions

Fig. 1 Schematic diagram of experimental apparatus.

1: Cylindrical plasma in discharge anode. 2: Discharge cathode. 3: H_2 or D_2 gas flow. 4: Discharge power supply. 5: Electron acceleration power supply. 6: Vacuum pump. 7: Area where cylindrical plasma is transformed into sheet plasma. 8: Insulation tube. 9: A pair of permanent magnets. 10: Magnetic field coils. 11: slit of electron acceleration anode. 12: Electron acceleration anode. 13: Floated end electrode. I_A: Current to electron acceleration anode. CP: Cylindrical plasma. SP: Sheet plasma. B_Z: Magnetic field. L: First extraction electrode. M: Second extraction electrode. E: Final extraction electrode. V_M: Potential of second extraction electrode with respect to electron acceleration anode. V_E: Potential of final extraction electrode with respect to electron acceleration anode. I_E: Negative current to final extraction electrode. MA: Magnetic deflection (90°) mass analyzer. B_M: Magnetic field intensity of MA. BC: Beam collector of MA. V_{BC}: Positive potential of BC with respect to MA. I^-: Negative current to BC. I_{MA}: Total negative current to MA. H_0^-: Hydrogen negative ions outside of sheet plasma. H^-: Accelerated hydrogen negative ions. π_0^-: Negative pionlike particles outside of sheet plasma. π^-: Accelerated negative pionlike particles.

Fig. 1 MA and Fig. 2 MA Schematic diagrams of mass analyzer M.A. and the extraction electrodes E.M.L.

E: final extraction electrode (with an aperture of 3 mm in diameter). V_E: Applied voltage of E. I_E: Negative current to E. S: Entrance slit (3 mm × 10 mm) of M.A. Fe: shows Iron. C: Magnetic coil. (N): North pole of electro-magnet. (S): South pole. B_M: Analyzing magnetic field. B.C: Beam collector. I^-: Negative current to B.C. V_{BC}: Bias voltage of B.C. with respect to M.A. X: Entrance of uniform magnetic field. H^-: Hydrogen negative ion. π^-: Negative pionlike particle.

Fig. 3 MA Fringe magnetic field distribution at (1A of M.A. coil current).

B_M: Analyzing magnetic field of M.A. B_0: Uniform magnetic field inside of M.A. S: Entrance slit position. X: Entrance of uniform magnetic field.

Fig. 2 (A) First experimental condition (positive ions to the back of beam collector B.C. are interrupted perfectly).

Ins: Insulator behind B.C. + Ion: Positive ions in front of B.C.

(See Figure Captions of Fig. 1, Fig. 1 MA, Fig. 2 MA and Fig. 3 MA also).

Fig. 2 (B) Dependences of negative current I^- to B.C. on magnetic field intensity B_M of MA.

π^-: First peak of I^- corresponding to negative pionlike particle. H^-: Second peak of I^- corresponding to hydrogen negative ion. (1): beam collector bias voltage $V_{BC} = 0V$ with respect to MA. (2): $V_{BC} = 25V$.

Fig. 3 (A) Second experimental condition (positive ions exist around beam collector B.C.).

+Ion: Positive ions around B.C.

Fig. 3 (B) Dependences of I^- to B.C. on B_M of MA.

(π^-): Position of B_M for negative pionlike particle. H^-: Peak of I^- corresponding to hydrogen negative ion. (1): $V_{BC} = 0V$. (2): $V_{BC} = 200V$.

Fig. 4 (A) Third experimental condition (in addition to First experimental condition, a metal plate of 0.5 mm in thickness MP is put partially in front of B.C.).

Fig. 4 (B) Dependences of negative current I^- to B.C. on B_M of MA.

π^-: Peak of I^- corresponding to negative pionlike particle. (H^-): Position of B_M for negative hydrogen ion. (1): $V_{BC} = 0V$. (2): $V_{BC} = 25V$. (3): $V_{BC} = 50V$.

Fig. 5 (A) Forth experimental condition (in addition to First experimental condition, a metal plate MP is put to screen B.C. perfectly).

Fig. 5 (B) Dependences of negative current I^- to B.C. on B_M of MA.

(π^-): Position of B_M for π^-. (H^-): Position of B_M for H^-.

Appendix Figure Captions

Fig. A1 (A) Fifth (previous) experimental condition (in addition to Second experimental condition, two insulators Ins are put behind B.C.).

Fig. A1 (B) Dependence of negative current I^- to B.C. on B_M of MA.

π^-: First peak of I^- corresponding to negative pionlike particle. H^-: Second peak of I^- corresponding to hydrogen negative particle. (1): $V_{BC} = 0V$. (2): $V_{BC} = 25V$.

Fig. A2 (A) Sixth experimental condition (in addition to Second experimental condition, a partial insulator Ins is put behind B.C.).

Fig. A2 (B) Dependence of negative current I^- to B.C. on B_M of MA.

(π^-): Position of B_M for π^-. H^-: Peak of I^- corresponding to hydrogen negative ion. (1): $V_{BC} = 0V$. (2): $V_{BC} = 100V$.

Fig. A3 Practical insulator arrangement for dection of π^-.

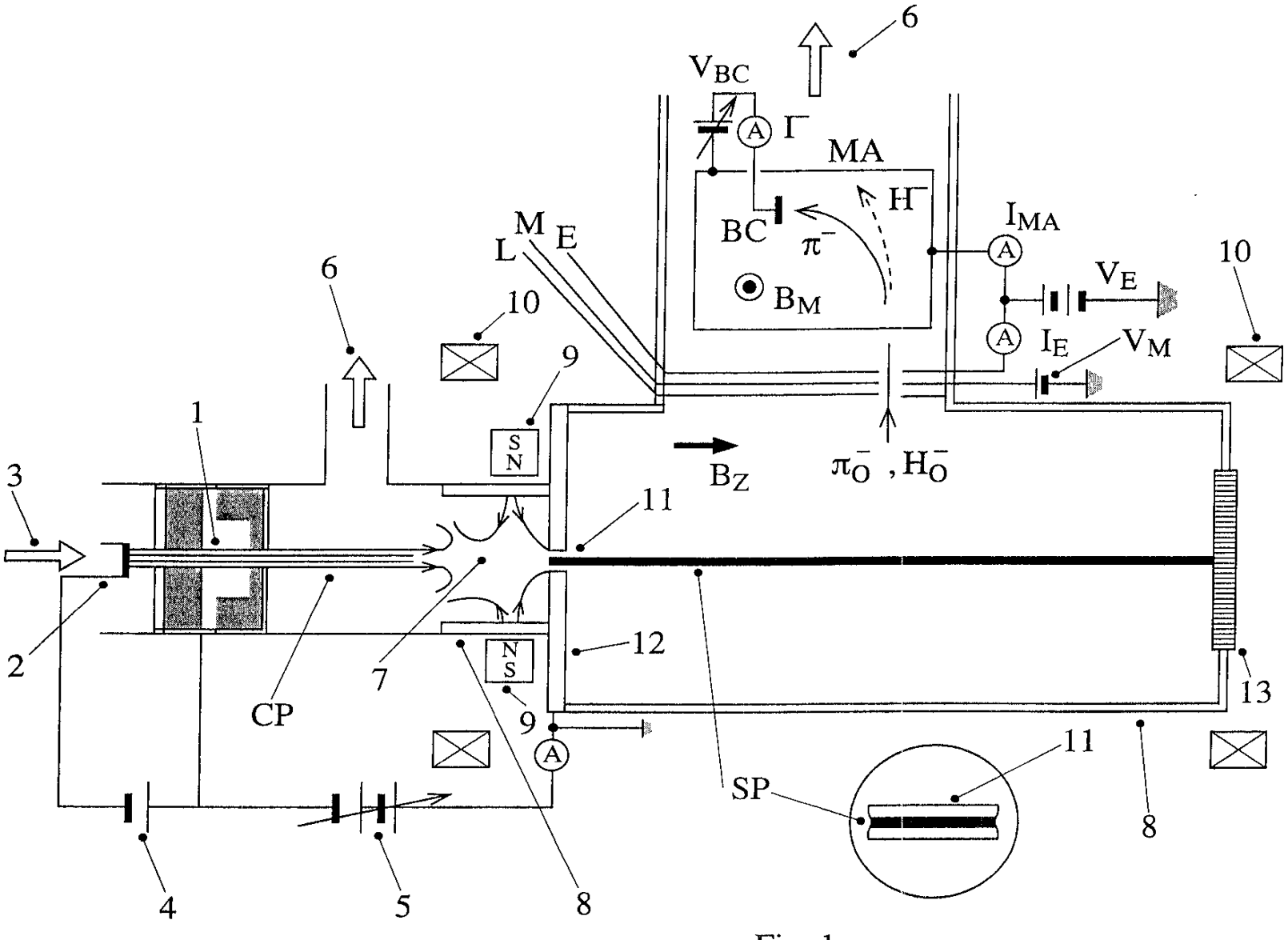
6
V_{BC}
A
I^-
MA
H^-
BC
π^-
B_M
I_{MA}
A
V_E
10
A
I_E
V_M
L
M
E
6
10
9
1
S
N
B_Z
π_O^- , H_O^-
3
11
2
CP
7
N
S
12
13
9
A
11
SP
8
4
5
8

Fig. 1

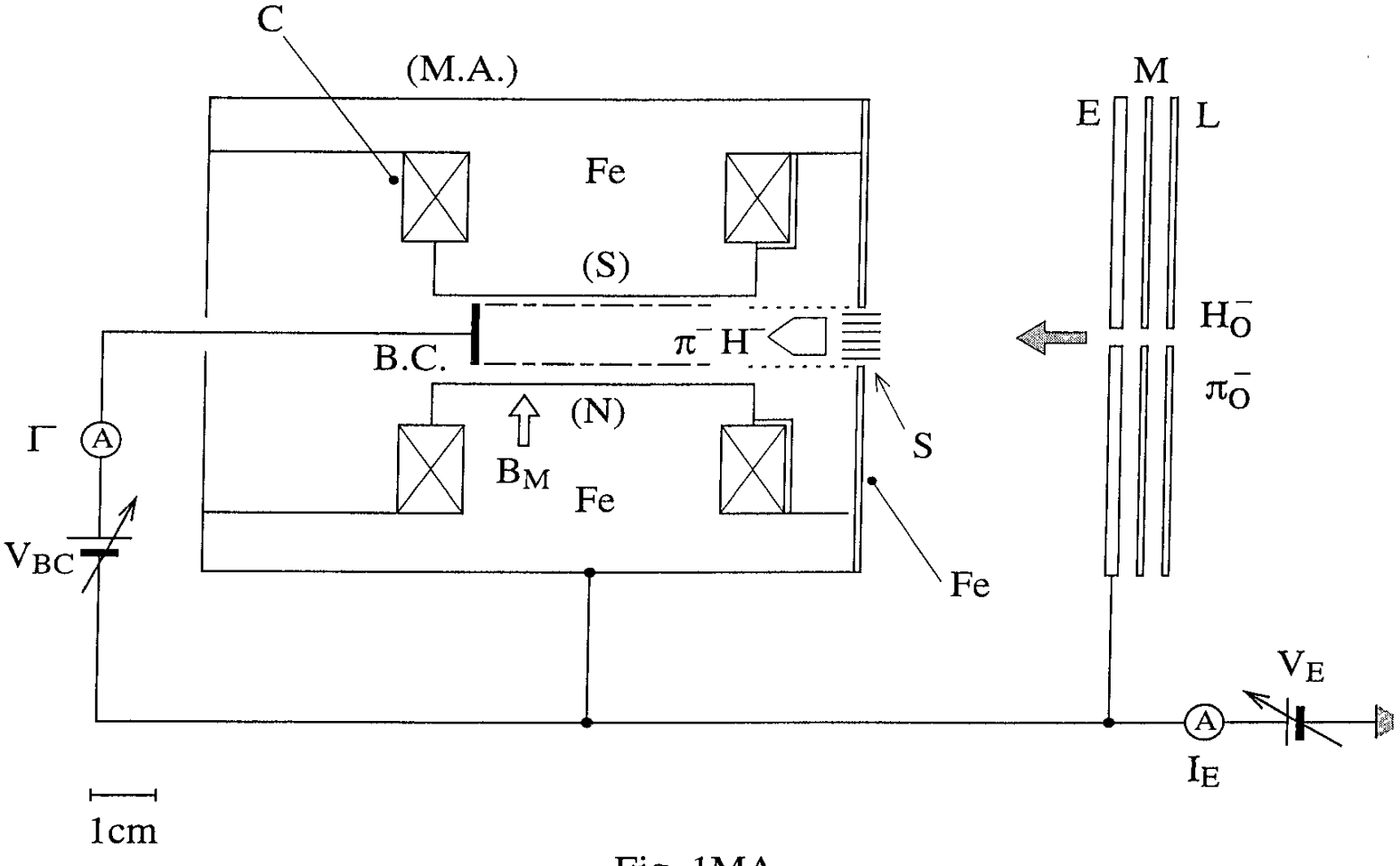

Fig. 1MA

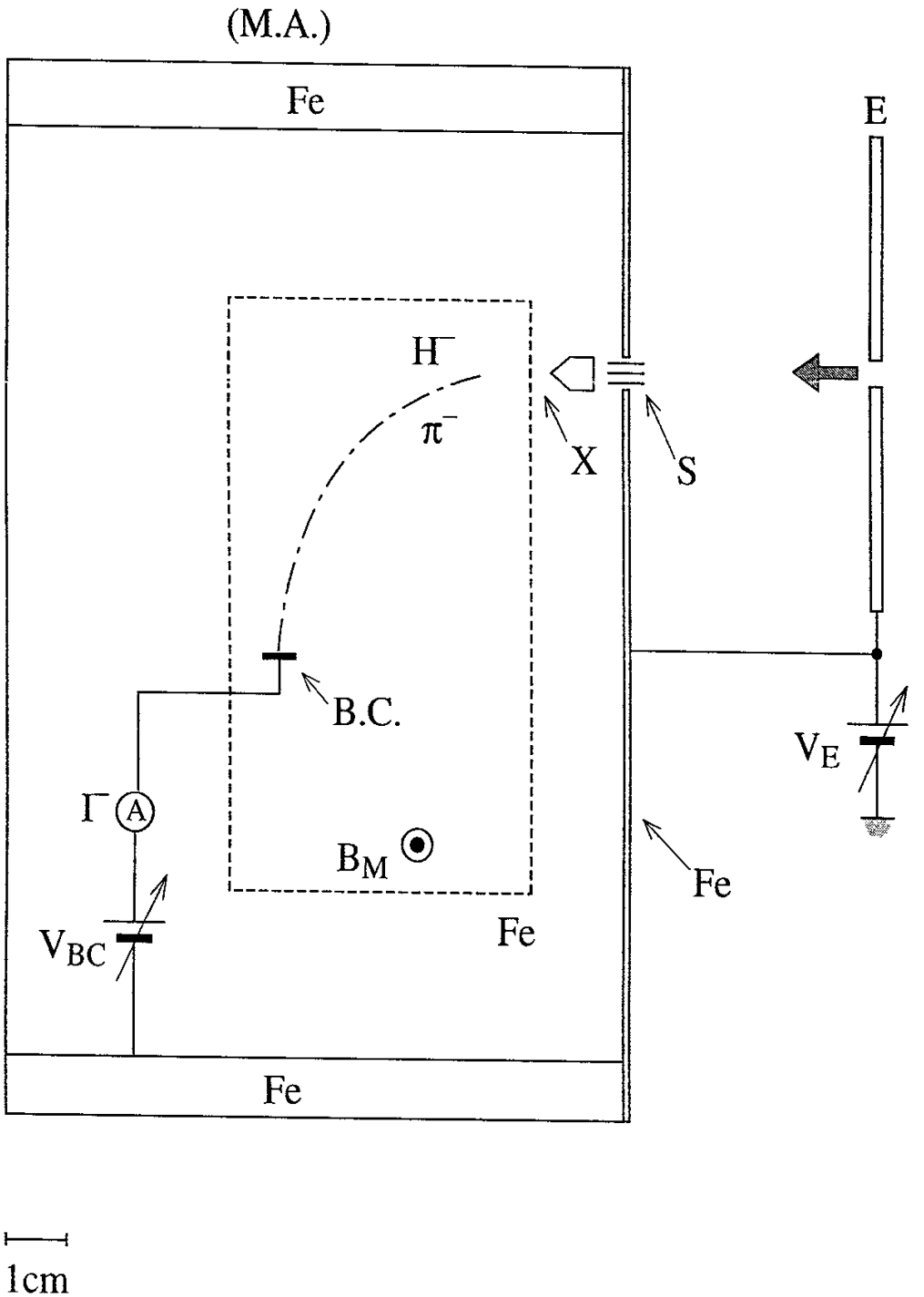

Fig. 2MA

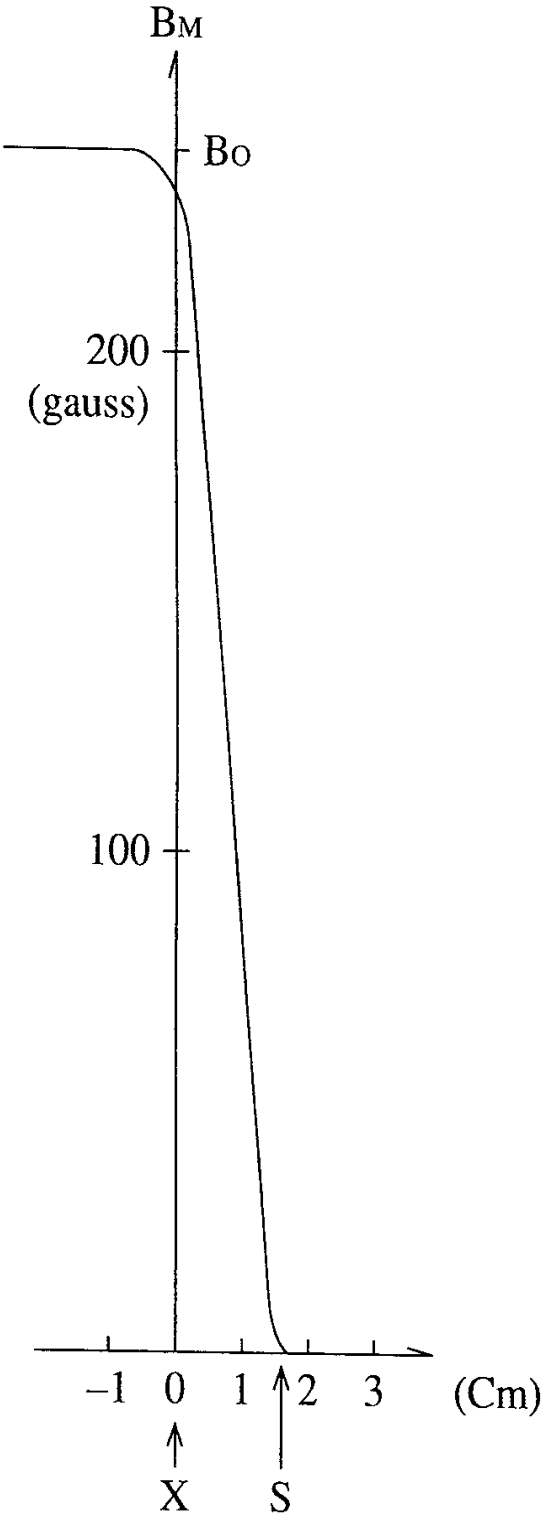

Fig. 3MA

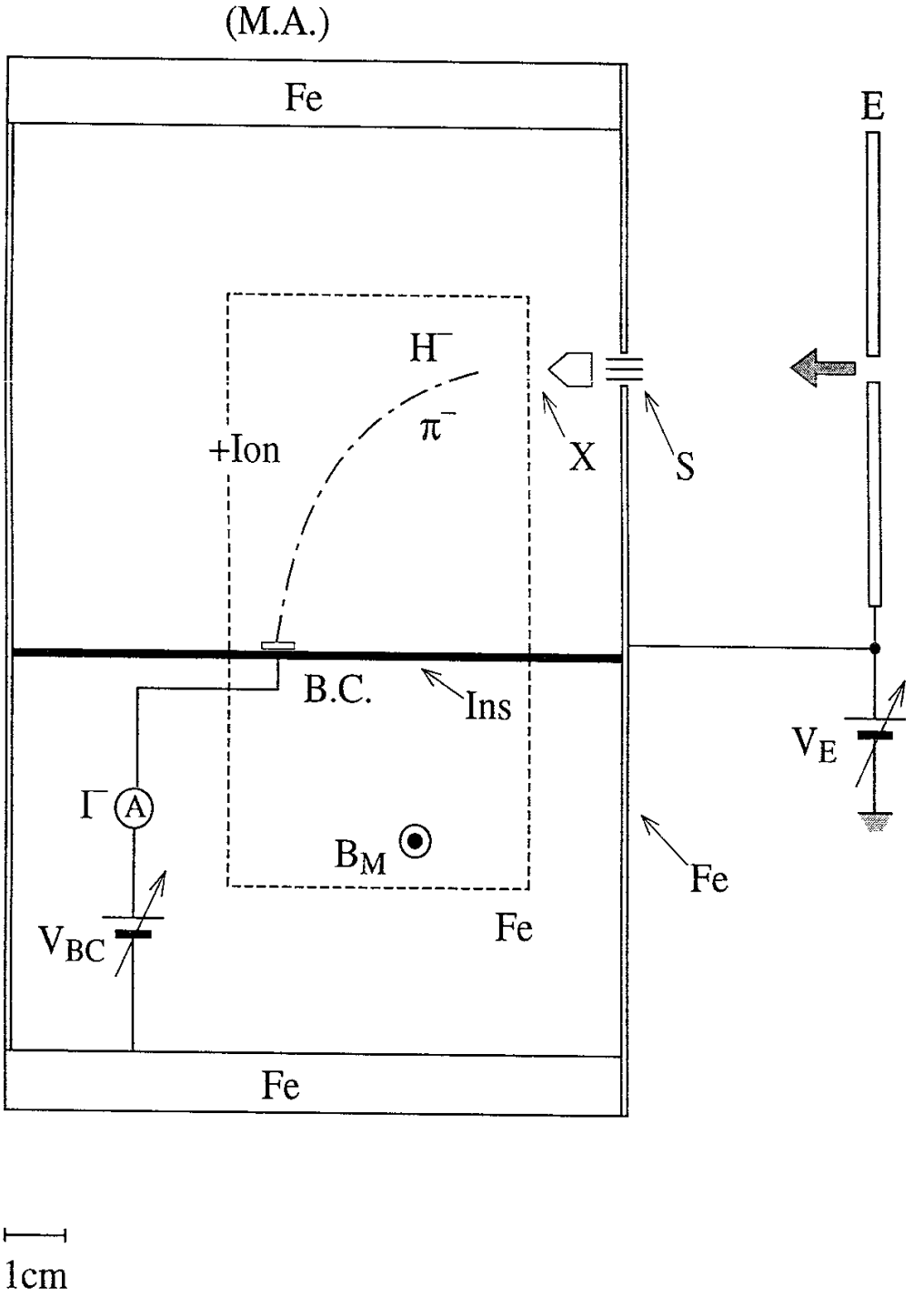

Fig. 2(A)

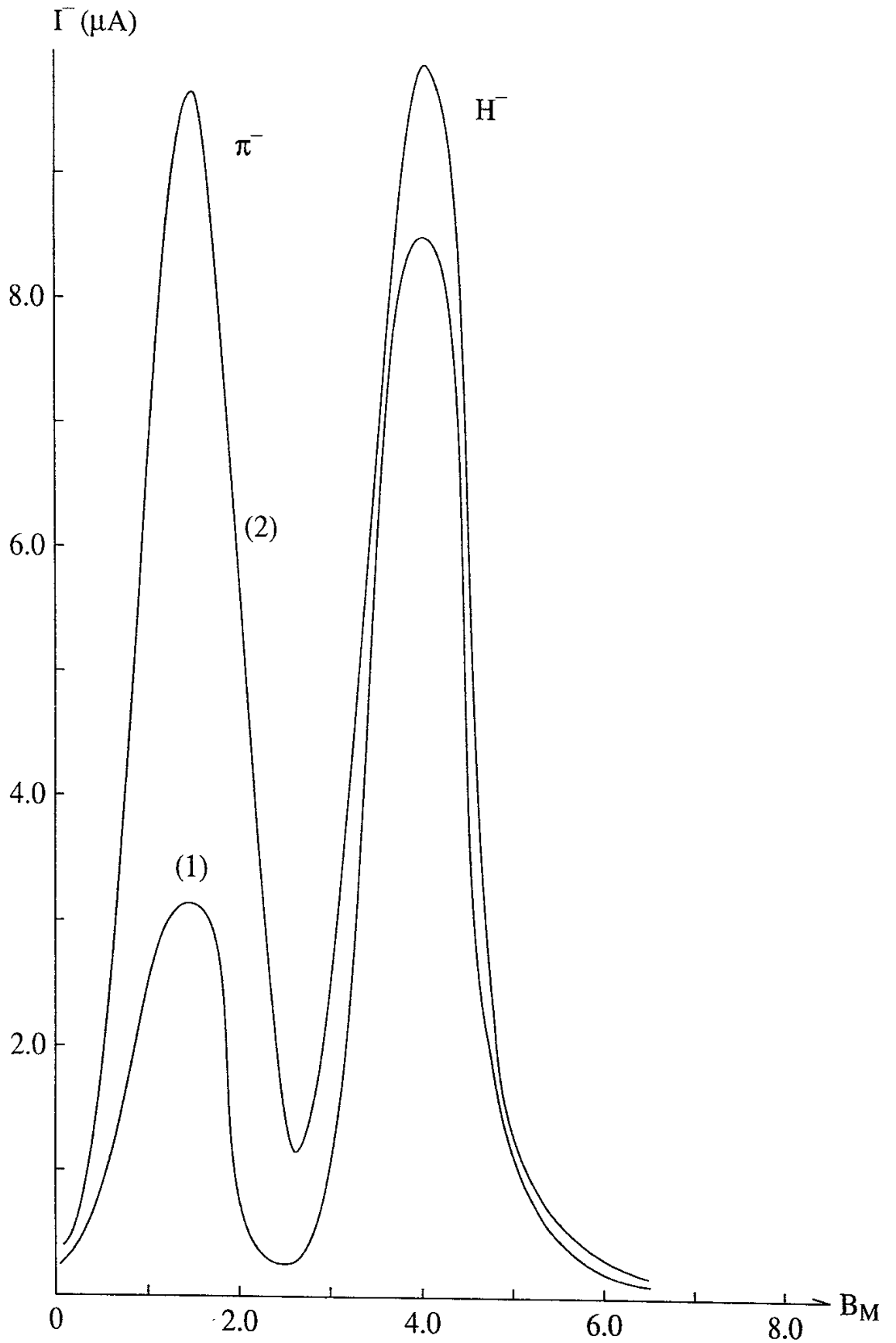

Fig. 2(B)

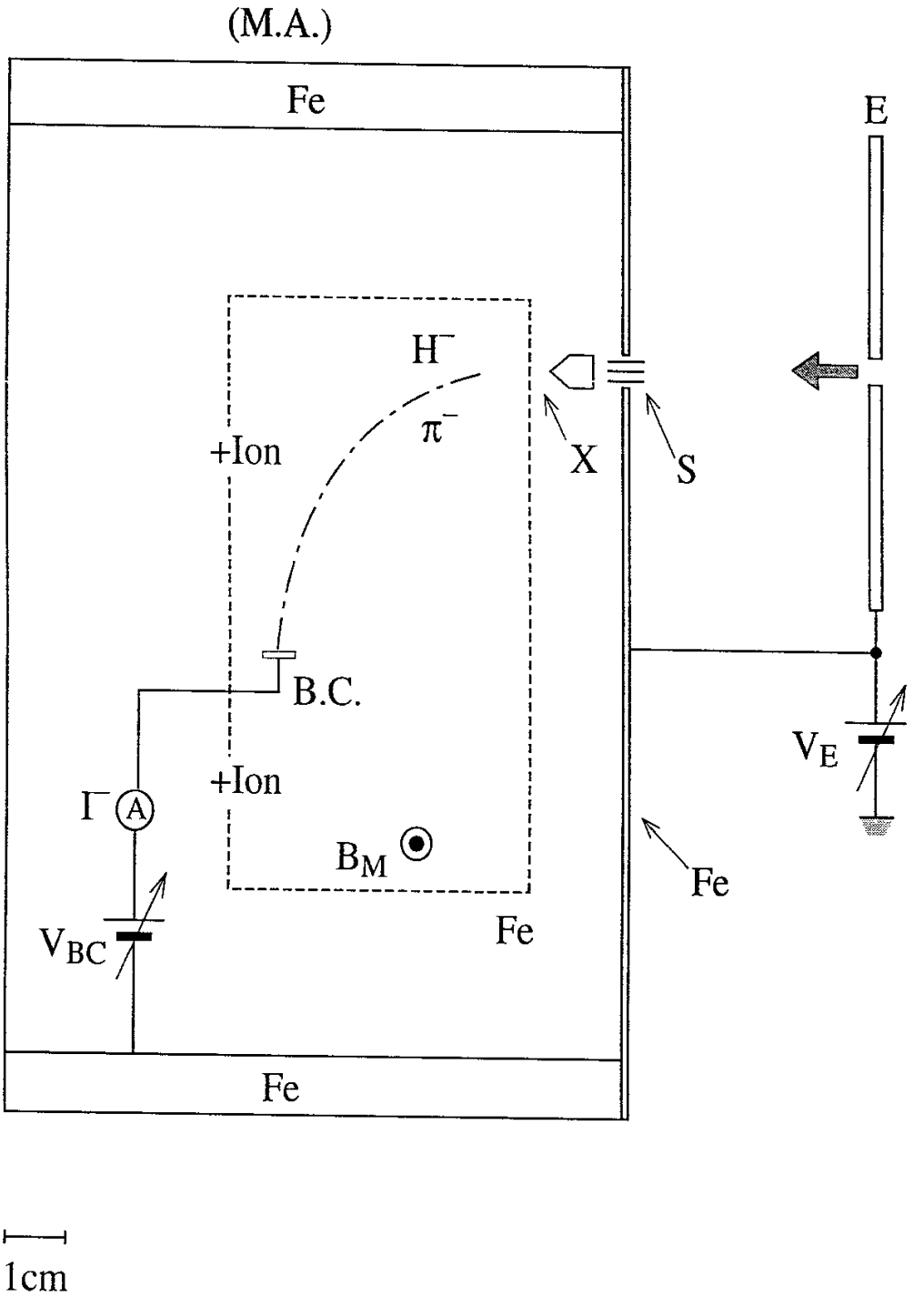

Fig. 3(A)

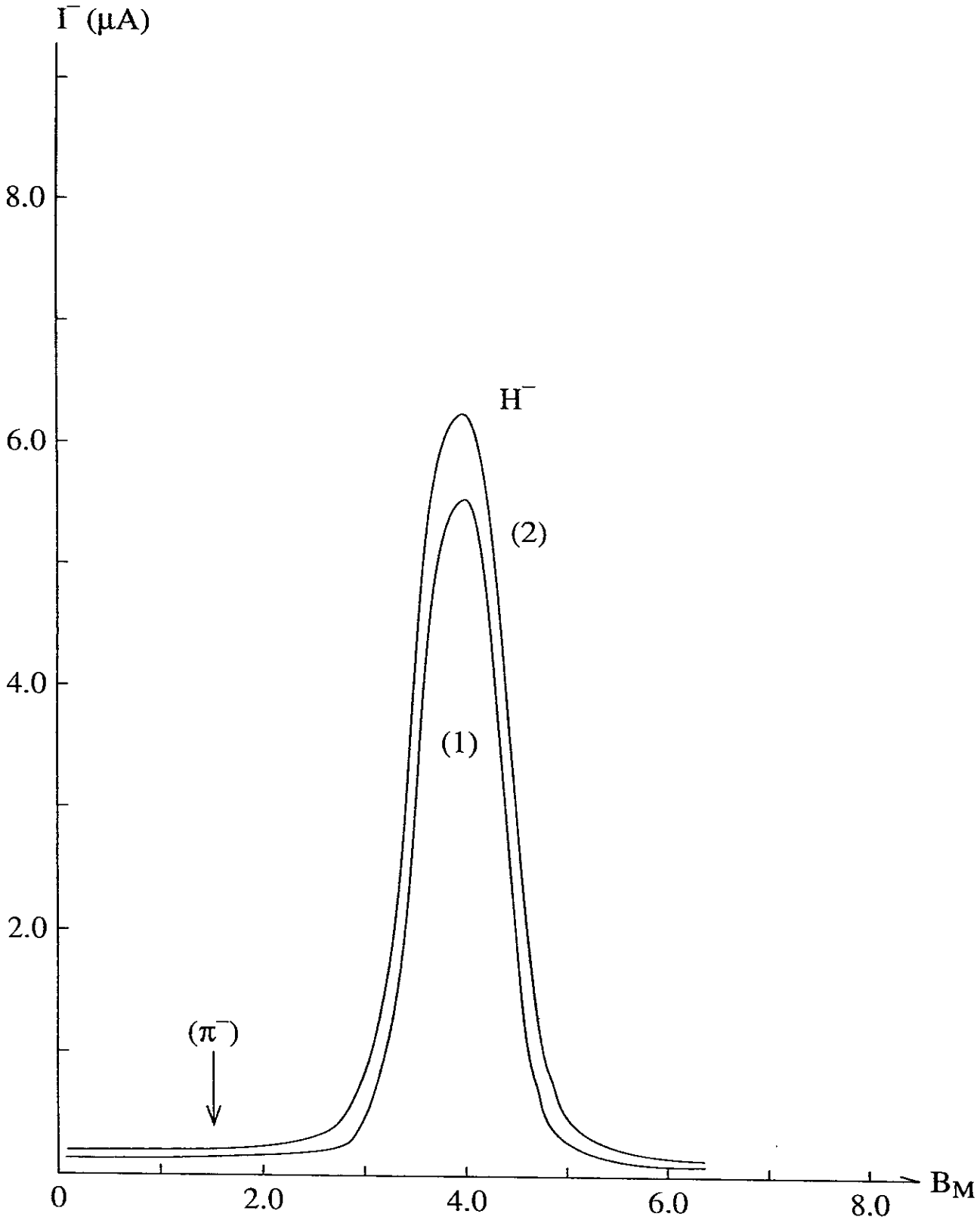

Fig. 3(B)

(×235 Gauss)

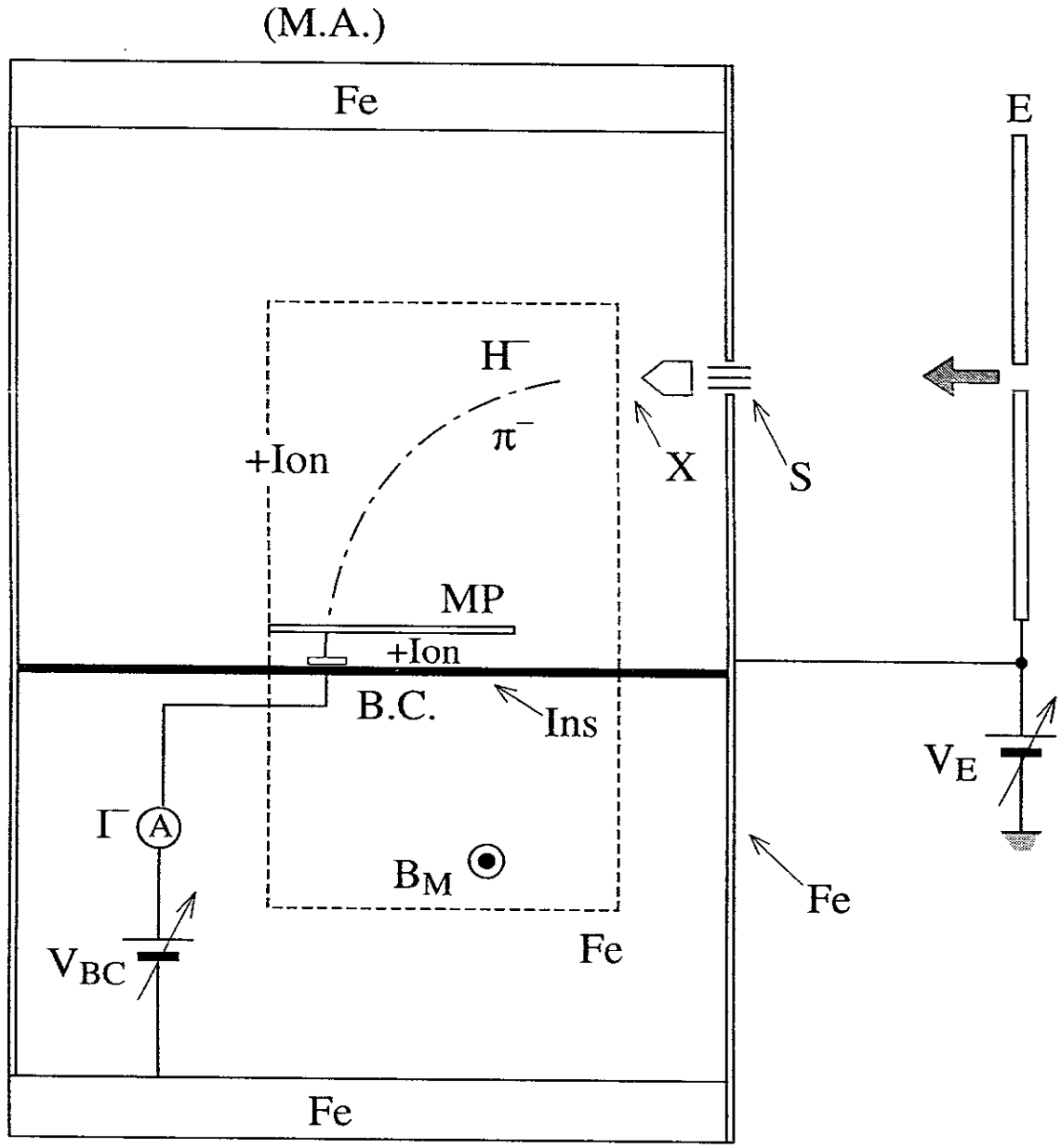

Fig. 4(A)

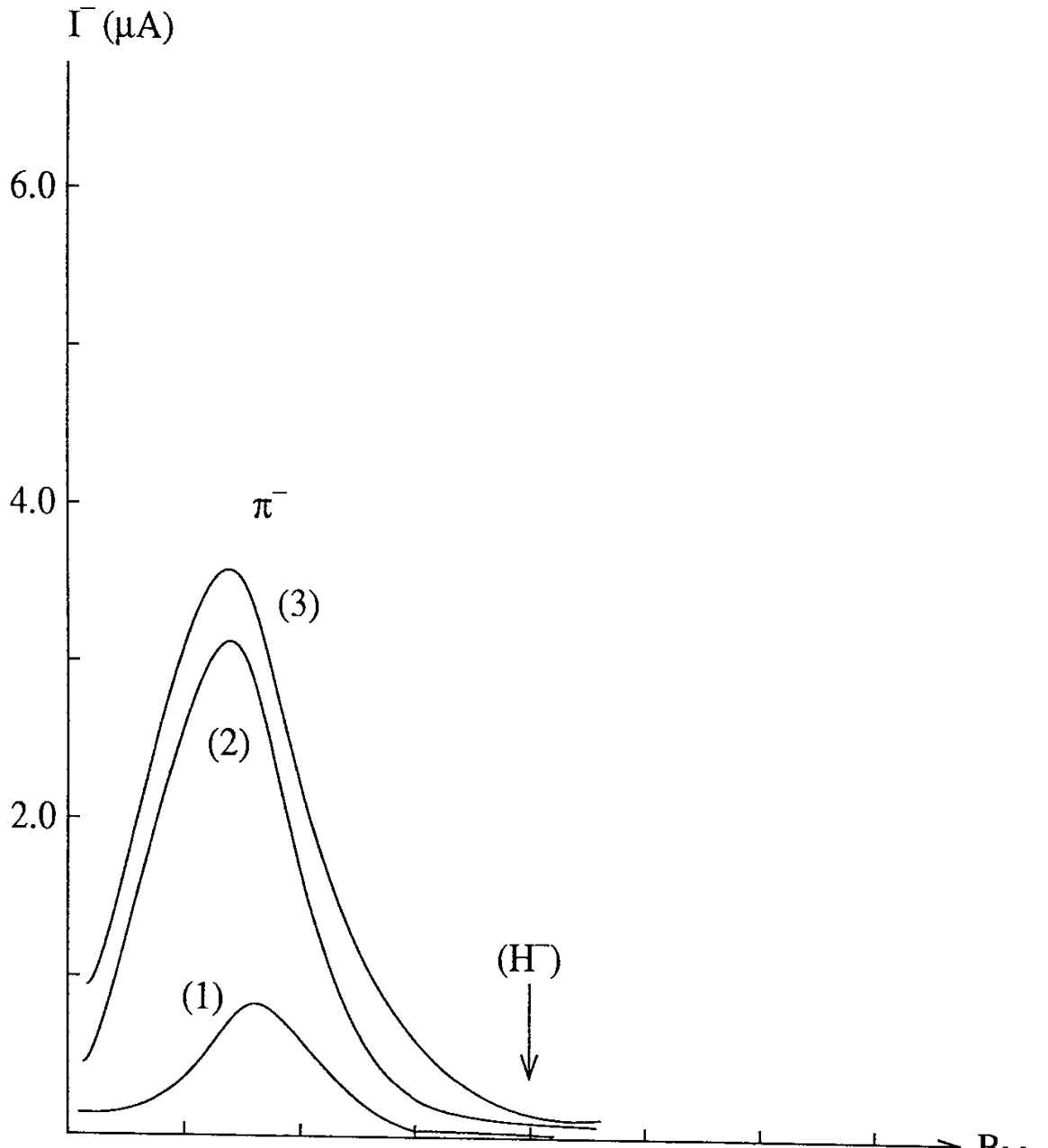

Fig. 4(B)

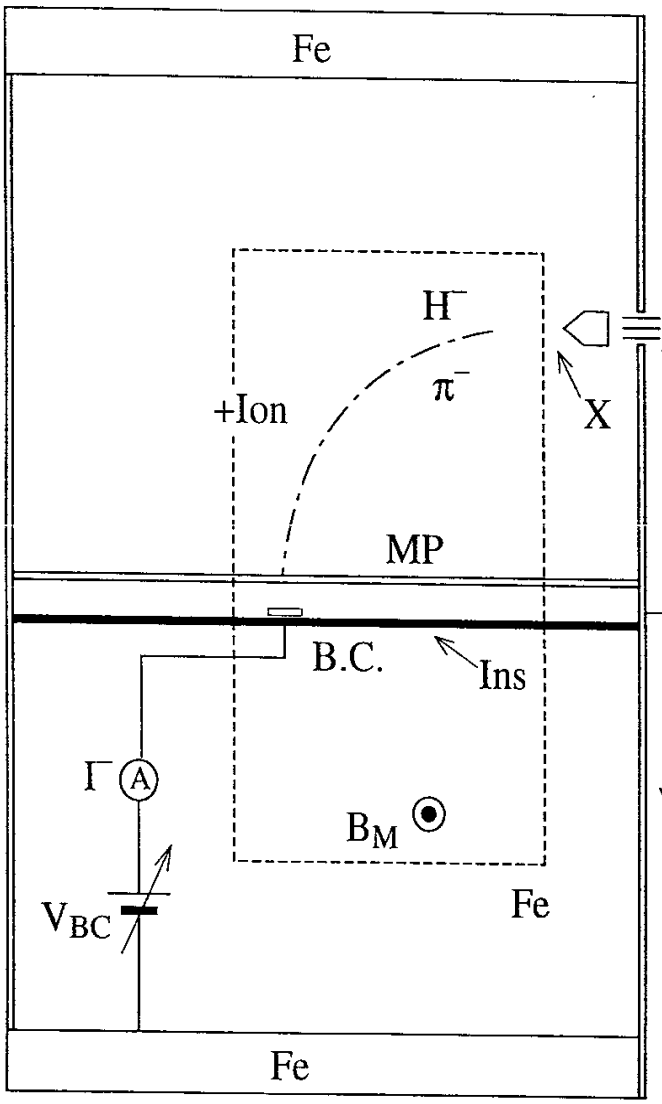
Fe
E
H⁻
π⁻
+Ion
X
S
MP
B.C.
Ins
I⁻ (μA)
I⁻
A
B_M
V_BC
V_E
Fe
Fe
Fe

Fig. 5(A)

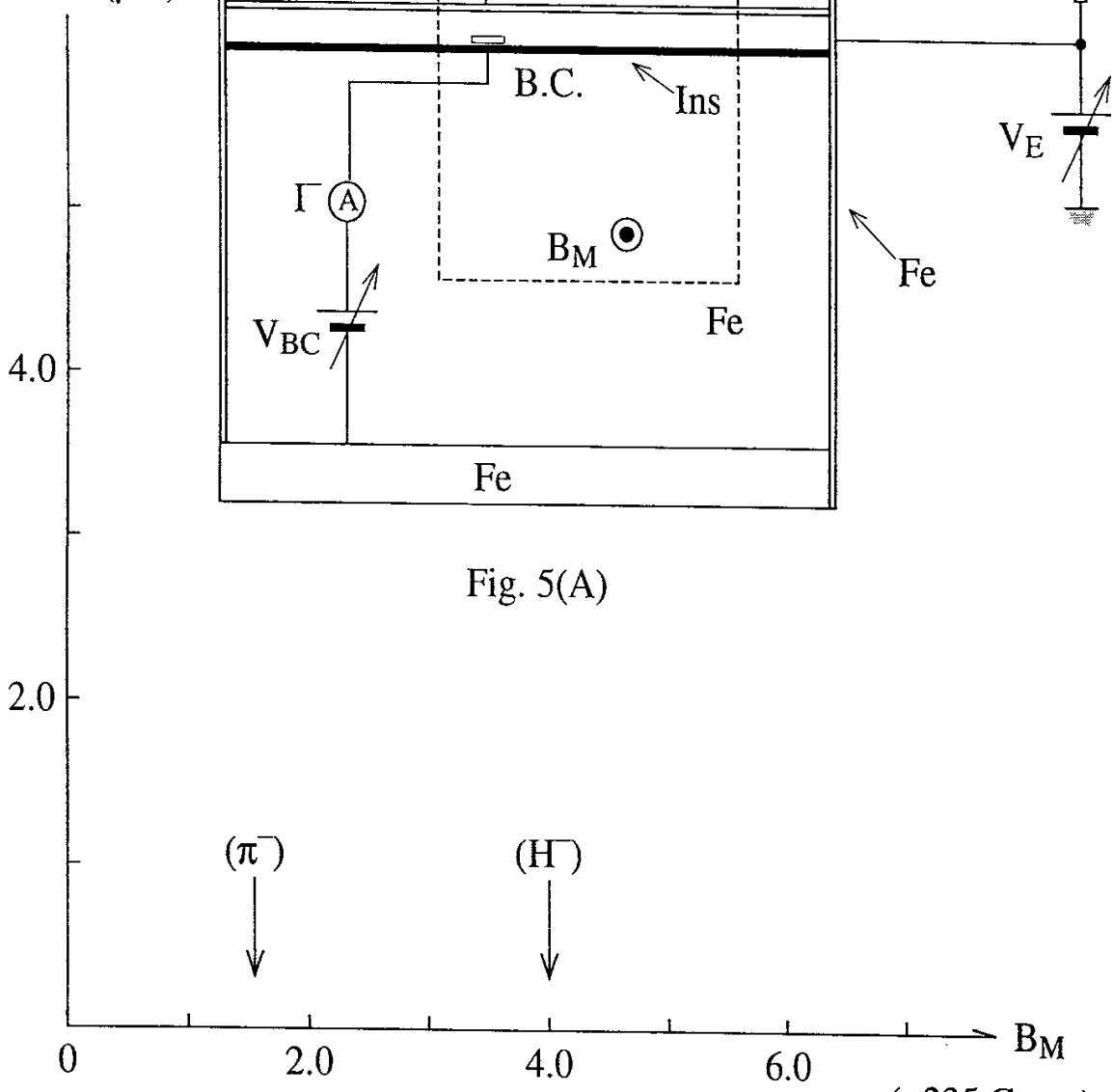
4.0
2.0
(π⁻)
(H⁻)
0
2.0
4.0
6.0
B_M
(×235 Gauss)

Fig. 5(B)

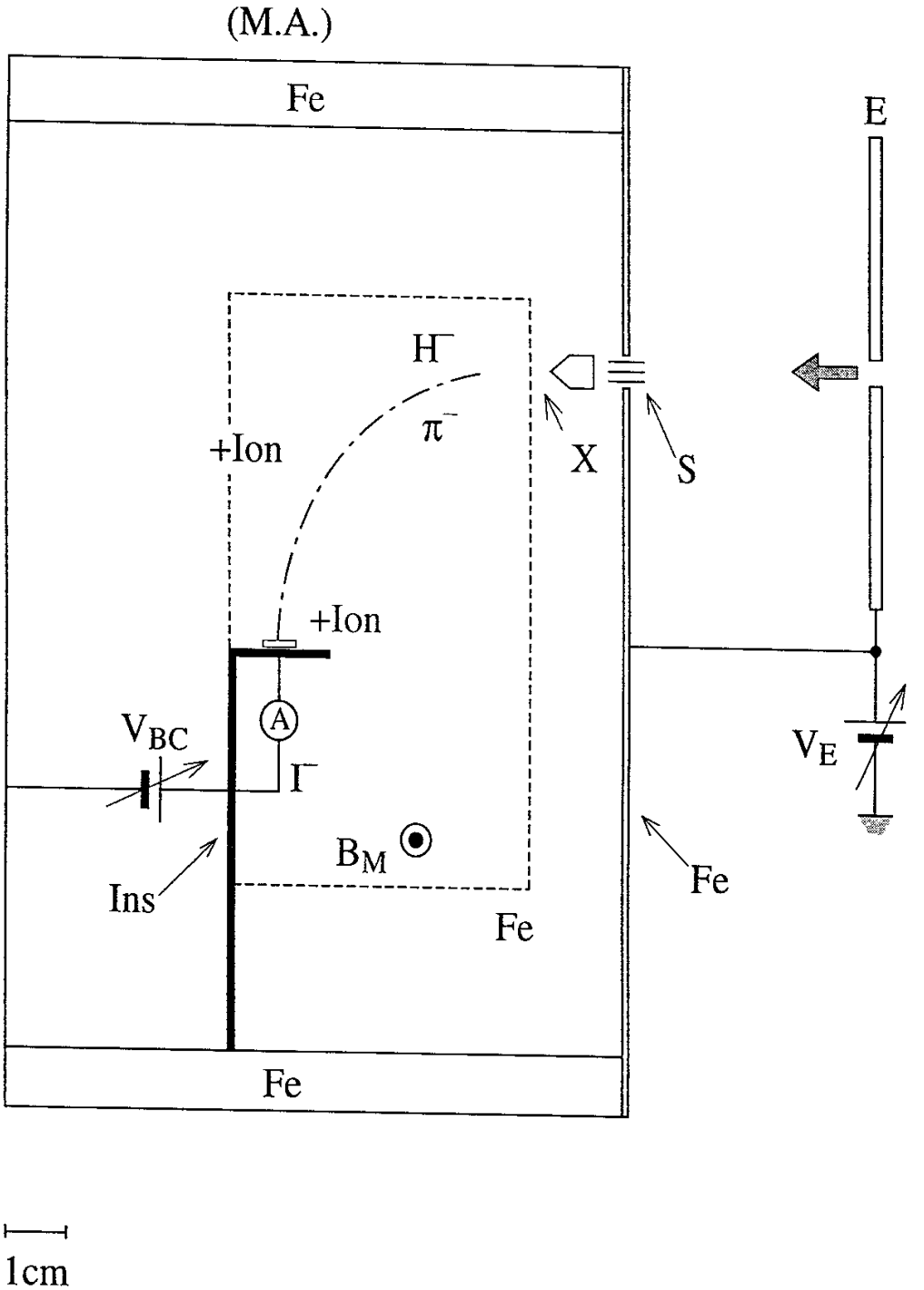

Fig. A1(A)

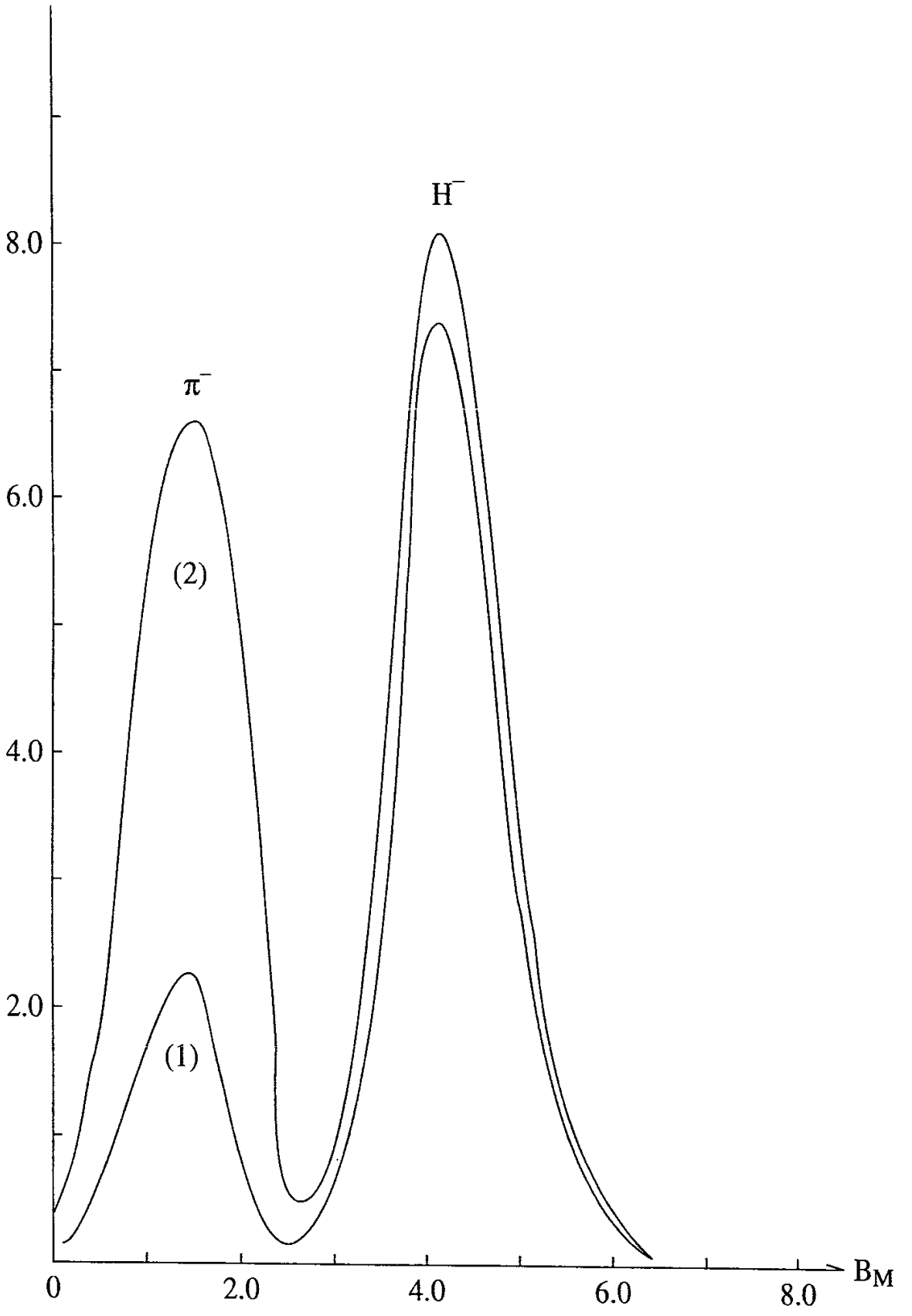

Fig. A1(B)

(×235 Gauss)

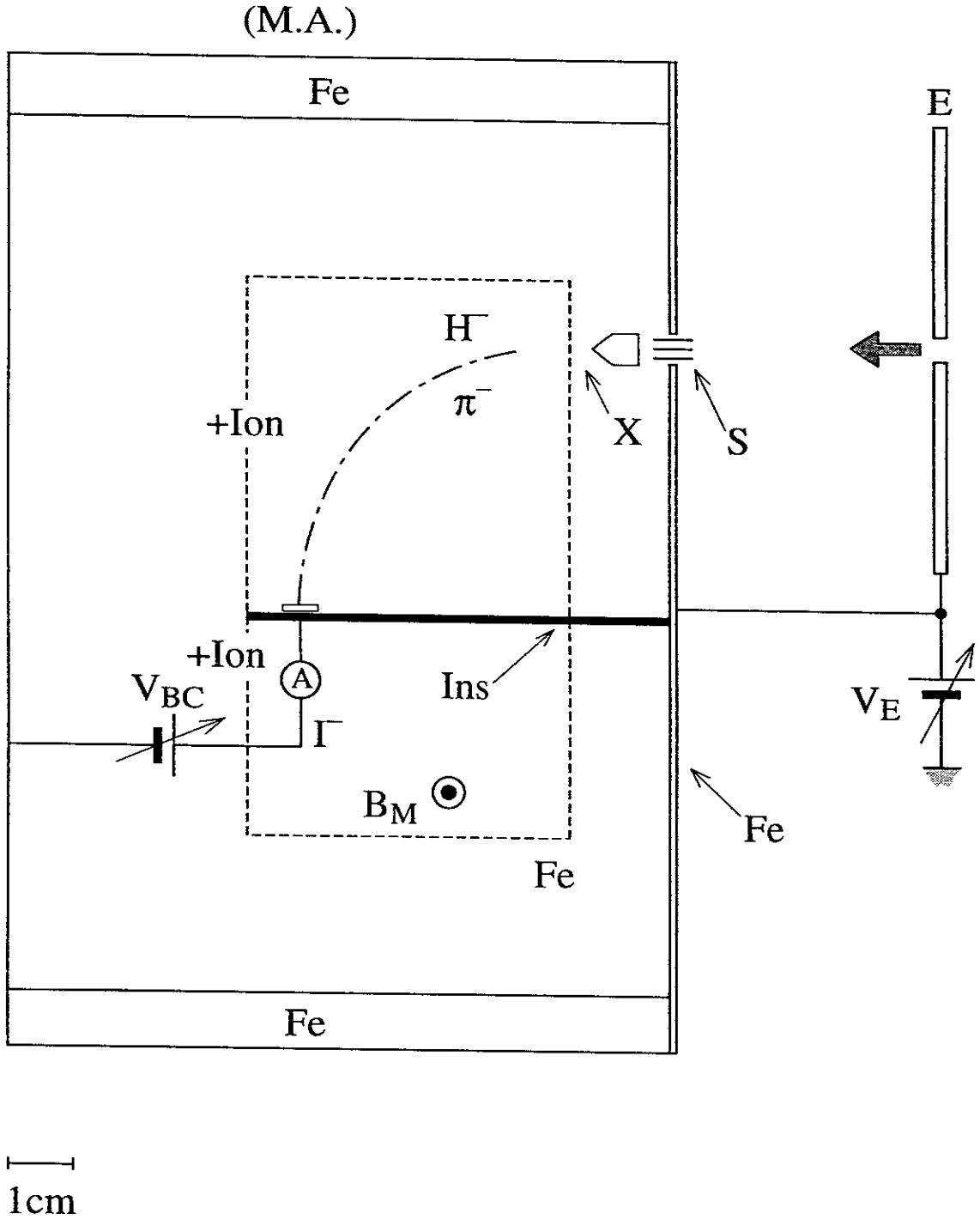

Fig. A2(A)

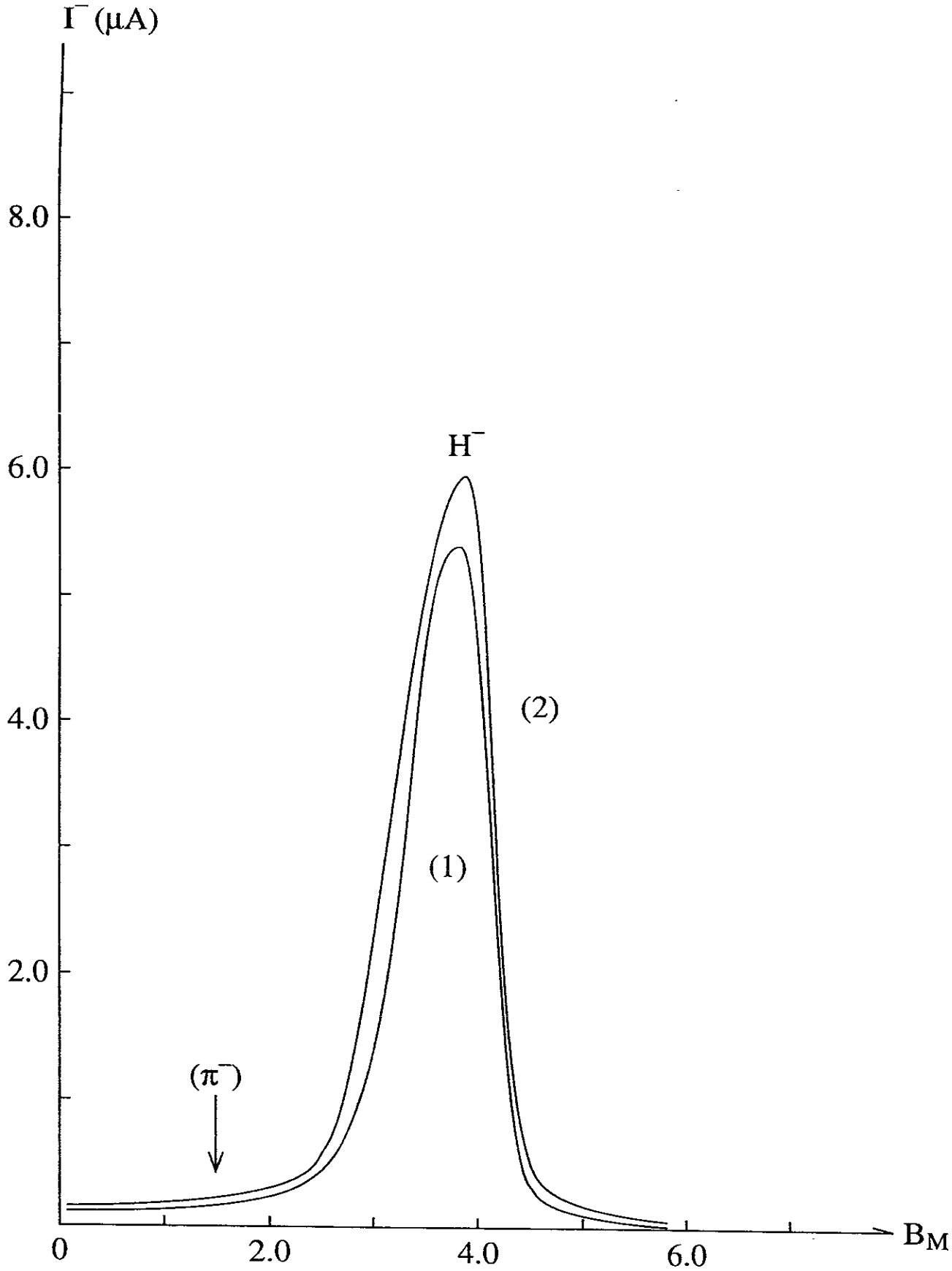

Fig. A2(B)

(×235 Gauss)

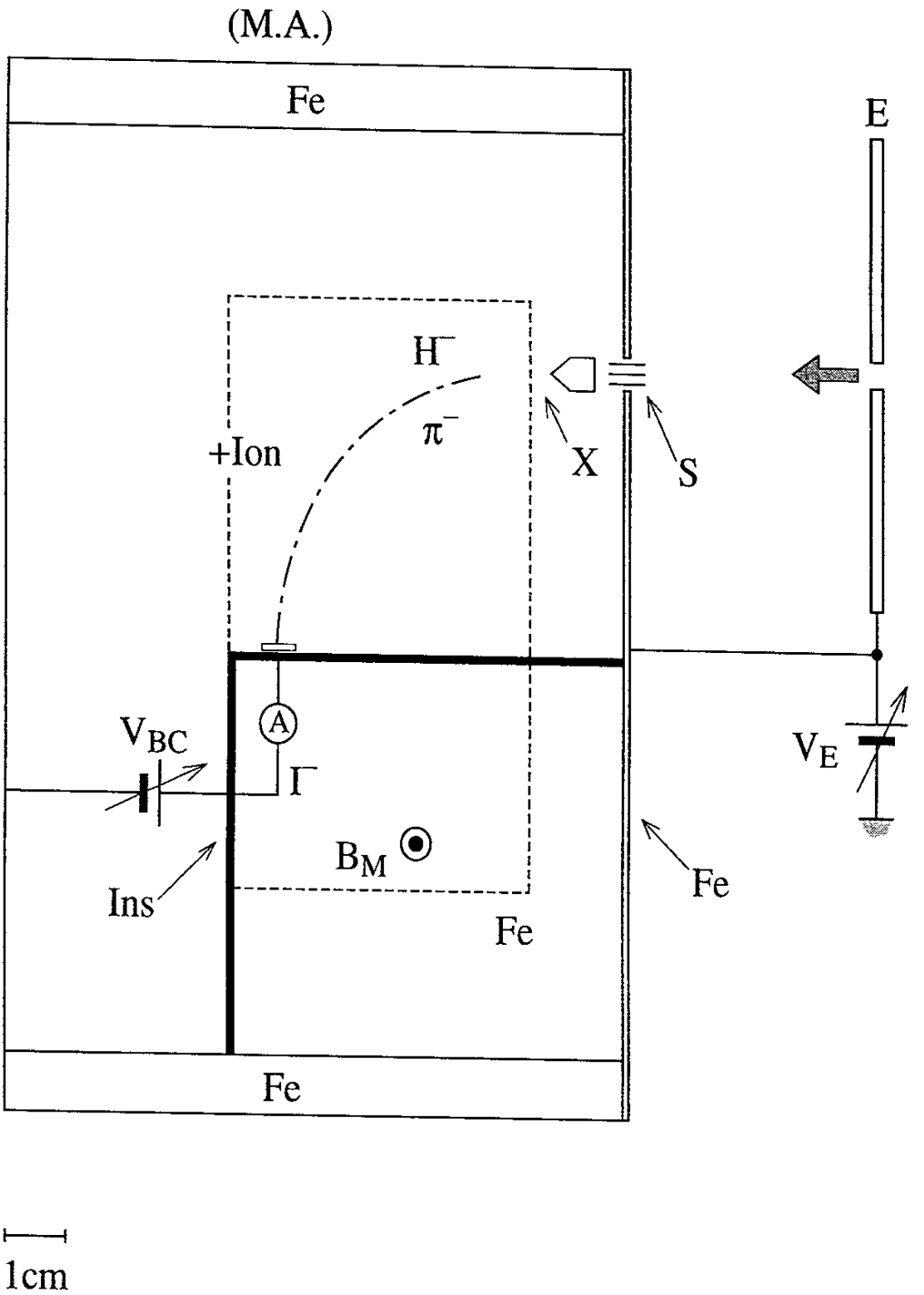

Fig. A3

Recent Issues of NIFS Series

NIFS-353 A. Nishizawa, Y. Hamada, Y. Kawasumi and H. Iguchi,
Increase of Lifetime of Thallium Zeolite Ion Source for Single-Ended Accelerator: May 1995

NIFS-354 S. Murakami, N. Nakajima, S. Okamura and M. Okamoto,
Orbital Aspects of Reachable β Value in NBI Heated Heliotron/Torsatrons; May 1995

NIFS-355 H. Sugama and W. Horton,
Neoclassical and Anomalous Transport in Axisymmetric Toroidal Plasmas with Electrostatic Turbulence; May 1995

NIFS-356 N. Ohyabu
A New Boundary Control Scheme for Simultaneous Achievement of H-mode and Radiative Cooling (SHC Boundary); May 1995

NIFS-357 Y. Hamada, K.N. Sato, H. Sakakita, A. Nishizawa, Y. Kawasumi, R. Liang, K. Kawahata, A. Ejiri, K. Toi, K. Narihara, K. Sato, T. Seki, H. Iguchi, A. Fujisawa, K. Adachi, S. Hidekuma, S. Hirokura, K. Ida, M. Kojima, J. Koong, R. Kumazawa, H. Kuramoto, T. Minami,. M. Sasao, T. Tsuzuki, J.Xu, I. Yamada, and T. Watari,
Large Potential Change Induced by Pellet Injection in JIPP T-IIU Tokamak Plasmas; May 1995

NIFS-358 M. Ida and T. Yabe,
Implicit CIP (Cubic-Interpolated Propagation) Method in One Dimension; May 1995

NIFS-359 A. Kageyama, T. Sato and The Complexity Simulation Group,
Computer Has Solved A Historical Puzzle: Generation of Earth's Dipole Field; June 1995

NIFS-360 K. Itoh, S.-I. Itoh, M. Yagi and A. Fukuyama,
Dynamic Structure in Self-Sustained Turbulence; June 1995

NIFS-361 K. Kamada, H. Kinoshita and H. Takahashi,
Anomalous Heat Evolution of Deuteron Implanted Al on Electron Bombardment; June 1995

NIFS-362 V.D. Pustovitov,
Suppression of Pfirsch-schlüter Current by Vertical Magnetic Field in Stellarators; June 1995

NIFS-363 A. Ida, H. Sanuki and J. Todoroki
An Extended K-dV Equation for Nonlinear Magnetosonic Wave in a Multi-Ion Plasma; June 1995

NIFS-364 H. Sugama and W. Horton
Entropy Production and Onsager Symmetry in Neoclassical Transport Processes of Toroidal Plasmas; July 1995

NIFS-365 K. Itoh, S.-I. Itoh, A. Fukuyama and M. Yagi,
On the Minimum Circulating Power of Steady State Tokamaks; July 1995

NIFS-366 K. Itoh and Sanae-I. Itoh,
The Role of Electric Field in Confinement; July 1995

NIFS-367 F. Xiao and T. Yabe,
A Rational Function Based Scheme for Solving Advection Equation; July 1995

NIFS-368 Y. Takeiri, O. Kaneko, Y. Oka, K. Tsumori, E. Asano, R. Akiyama, T. Kawamoto and T. Kuroda,
Multi-Beamlet Focusing of Intense Negative Ion Beams by Aperture Displacement Technique; Aug. 1995

NIFS-369 A. Ando, Y. Takeiri, O. Kaneko, Y. Oka, K. Tsumori, E. Asano, T. Kawamoto, R. Akiyama and T. Kuroda,
Experiments of an Intense H- Ion Beam Acceleration; Aug. 1995

NIFS-370 M. Sasao, A. Taniike, I. Nomura, M. Wada, H. Yamaoka and M. Sato,
Development of Diagnostic Beams for Alpha Particle Measurement on ITER; Aug. 1995

NIFS-371 S. Yamaguchi, J. Yamamoto and O. Motojima;
A New Cable -in conduit Conductor Magnet with Insulated Strands; Sep. 1995

NIFS-372 H. Miura,
Enstrophy Generation in a Shock-Dominated Turbulence; Sep. 1995

NIFS-373 M. Natsir, A. Sagara, K. Tsuzuki, B. Tsuchiya, Y. Hasegawa, O. Motojima,
Control of Discharge Conditions to Reduce Hydrogen Content in Low Z Films Produced with DC Glow; Sep. 1995

NIFS-374 K. Tsuzuki, M. Natsir, N. Inoue, A. Sagara, N. Noda, O. Motojima, T. Mochizuki, I. Fujita, T. Hino and T. Yamashina,
Behavior of Hydrogen Atoms in Boron Films during H_2 and He Glow Discharge and Thermal Desorption; Sep. 1995

NIFS-375 U. Stroth, M. Murakami, R.A. Dory, H. Yamada, S. Okamura, F. Sano and T. Obiki,
Energy Confinement Scaling from the International Stellarator Database; Sep. 1995

NIFS-376 S. Bazdenkov, T. Sato, K. Watanabe and The Complexity Simulation Group, *Multi-Scale Semi-Ideal Magnetohydrodynamics of a Tokamak Plasma;* Sep. 1995

NIFS-377 J. Uramoto, *Extraction of Negative Pionlike Particles from a H2 or D2 Gas Discharge Plasma in Magnetic Field;* Sep. 1995

NIFS-378 K. Akaishi, *Theoretical Consideration for the Outgassing Characteristics of an Unbaked Vacuum System*; Oct. 1995

NIFS-379 H. Shimazu, S. Machida and M. Tanaka, *Macro-Particle Simulation of Collisionless Parallel Shocks*; Oct. 1995

NIFS-380 N. Kondo and Y. Kondoh, *Eigenfunction Spectrum Analysis for Self-organization in Dissipative Solitons;* Oct. 1995

NIFS-381 Y. Kondoh, M. Yoshizawa, A. Nakano and T. Yabe, *Self-organization of Two-dimensional Incompressible Viscous Flow in a Friction-free Box;* Oct. 1995

NIFS-382 Y.N. Nejoh and H. Sanuki, *The Effects of the Beam and Ion Temperatures on Ion-Acoustic Waves in an Electron Beam-Plasma System;* Oct. 1995

NIFS-383 K. Ichiguchi, O. Motojima, K. Yamazaki, N. Nakajima and M. Okamoto *Flexibility of LHD Configuration with Multi-Layer Helical Coils;* Nov. 1995

NIFS-384 D. Biskamp, E. Schwarz and J.F. Drake, *Two-dimensional Electron Magnetohydrodynamic Turbulence*; Nov. 1995

NIFS-385 H. Kitabata, T. Hayashi, T. Sato and Complexity Simulation Group, *Impulsive Nature in Collisional Driven Reconnection*; Nov. 1995

NIFS-386 Y. Katoh, T. Muroga, A. Kohyama, R.E. Stoller, C. Namba and O. Motojima, *Rate Theory Modeling of Defect Evolution under Cascade Damage Conditions:The Influence of Vacancy-type Cascade Remnants and Application to the Defect Production Chracterization by Microstructural Analysis;* Nov. 1995

NIFS-387 K. Araki, S. Yanase and J. Mizushima, *Symmetry Breaking by Differential Rotation and Saddle-node Bifurcation of the Thermal Convection in a Spherical Shell*; Dec. 1995

NIFS-388 V.D. Pustovitov,

Control of Pfirsch-Schlüter Current by External Poloidal Magnetic Field in Conventional Stellarators: Dec. 1995

NIFS-389 K. Akaishi,
On the Outgassing Rate Versus Time Characteristics in the Pump-down of an Unbaked Vacuum System; Dec. 1995

NIFS-390 K.N. Sato, S. Murakami, N. Nakajima, K. Itoh,
Possibility of Simulation Experiments for Fast Particle Physics in Large Helical Device (LHD); Dec. 1995

NIFS-391 W.X.Wang, M. Okamoto, N. Nakajima, S. Murakami and N. Ohyabu,
A Monte Carlo Simulation Model for the Steady-State Plasma in the Scrape-off Layer; Dec. 1995

NIFS-392 Shao-ping Zhu, R. Horiuchi, T. Sato and The Complexity Simulation Group,
Self-organization Process of a Magnetohydrodynamic Plasma in the Presence of Thermal Conduction; Dec. 1995

NIFS-393 M. Ozaki, T. Sato, R. Horiuchi and the Complexity Simulation Group
Electromagnetic Instability and Anomalous Resistivity in a Magnetic Neutral Sheet; Dec. 1995

NIFS-394 K. Itoh, S.-I Itoh, M. Yagi and A. Fukuyama,
Subcritical Excitation of Plasma Turbulence; Jan. 1996

NIFS-395 H. Sugama and M. Okamoto, W. Horton and M. Wakatani,
Transport Processes and Entropy Production in Toroidal Plasmas with Gyrokinetic Eletromagnetic Turbulence; Jan. 1996

NIFS-396 T. Kato, T. Fujiwara and Y. Hanaoka,
X-ray Spectral Analysis of Yohkoh BCS Data on Sep. 6 1992 Flares - Blue Shift Component and Ion Abundances -; Feb. 1996

NIFS-397 H. Kuramoto, N. Hiraki, S. Moriyama, K. Toi, K. Sato, K. Narihara, A. Ejiri, T. Seki and JIPP T-IIU Group,
Measurement of the Poloidal Magnetic Field Profile with High Time Resolution Zeeman Polarimeter in the JIPP T-IIU Tokamak; Feb. 1996

NIFS-398 J.F. Wang, T. Amano, Y. Ogawa, N. Inoue,
Simulation of Burning Plasma Dynamics in ITER; Feb. 1996

NIFS-399 K. Itoh, S-I. Itoh, A. Fukuyama and M. Yagi,
Theory of Self-Sustained Turbulence in Confined Plasmas; Feb. 1996

NIFS-400 J. Uramoto,
A Detection Method of Negative Pionlike Particles from a H2 Gas Descharge Plasma; Feb. 1996